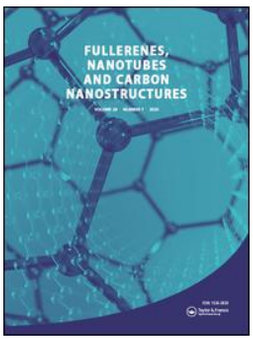

Taylor & Francis
Taylor & Francis Group

Fullerenes, Nanotubes and Carbon Nanostructures

ISSN: (Print) (Online) Journal homepage: https://www.tandfonline.com/loi/lfnn20

A review on C1s XPS-spectra for some kinds of carbon materials

Xiangnan Chen , Xiaohui Wang & De Fang

To cite this article: Xiangnan Chen , Xiaohui Wang & De Fang (2020): A review on C1s XPS-spectra for some kinds of carbon materials, Fullerenes, Nanotubes and Carbon Nanostructures, DOI: 10.1080/1536383X.2020.1794851

To link to this article: https://doi.org/10.1080/1536383X.2020.1794851

Published online: 21 Jul 2020.

FULLERENES, NANOTUBES AND CARBON NANOSTRUCTURES
https://doi.org/10.1080/1536383X.2020.1794851

A review on C1s XPS-spectra for some kinds of carbon materials

Xiangnan Chen[a], Xiaohui Wang[a,b], and De Fang[a,b,c]

[a]School of Materials Science and Engineering, Wuhan University of Technology, Wuhan, PR China; [b]State Key Laboratory of Silicate Materials for Architectures, Wuhan University of Technology, Wuhan, PR China; [c]Center for Materials Research and Analysis, Wuhan University of Technology, Wuhan, PR China

ABSTRACT

The surface properties of carbon materials are very important since many complex physical and chemical reactions take place on their surfaces. X-ray photoelectron spectroscopy (XPS) test is one of the most significant characterization methods to analyze the surfaces. The carbon species and banding energies for several typical kinds of carbon materials (graphite, carbon black, graphene, carbon nanotubes, carbides, and polymers) were summarized with typical XPS spectra. It can be found that carbon materials with different preparation methods, analytical methods or storage times possess quite different carbon species and banding energies. Meanwhile, classical XPS figures and analysis results of every carbon material were illustrated, which provides the researchers an intuitive understanding of the related analytical method. Therefore, much more accurate results of XPS spectra for related carbon materials can be obtained.

ARTICLE HISTORY
Received 8 July 2020
Accepted 9 July 2020

KEYWORDS
XPS; surface; carbon materials; carbon species; banding energies

1. Introduction

As significant important materials, carbon materials are widely used in the academic world.[1–4] They can be divided into two categories, while one is classic carbons (such as carbon blacks, activated carbon, coke, graphite, diamond) and another one is new carbons (such as carbon fibers, porous carbons, glass-like carbons, carbon nanotubes, and graphene, fullerene). Their applications can be found in the fields of technical interest from nonlinear optics to sensors and catalysis since there are many oxygenated groups (such as carbonyl and carboxyl) on the surfaces of carbon materials. The properties of carbon materials on the surface require a more reliable and deeper understanding, when the surfaces are modified with abundant physical and chemical methods. adding functional groups. And the characterization of surface functionalities for carbon materials is important in identifying and controlling the surface structure. As a surface analysis technique, X-ray photoelectron spectroscopy (XPS) has been extremely useful to analyze surface chemical states of C1s XPS-spectra for carbon materials in the scientific researches,[5–9] while the most notable of many features for XPS is the surface sensitivity.[10–12] It has been found that the selected carbon material shows quite different XPS peaks due to the factors such as the storage period, preparation method, instrument resolution, analytical method and so on. Moreover, in relevant published references, the analytical method is either not given or not correct for different carbon species and banding energies. Therefore, it is necessary to analyze and summarize the relative literatures of carbon materials.

In this paper, surface chemical states of C1s XPS-spectra for several typical kinds of carbon materials (graphite, carbon black, graphene, carbon nanotubes, carbides, and polymers) are shown with the literatures. The kinds of bonds related to carbon are listed and the binding energies for the C1s peaks are summarized, which is extremely convenient for the researchers get information about the types of carbon.

2. Typical carbon materials

2.1. Graphite

Graphite is crystalline elemental carbon, which is one of the longest-known forms of pure carbon.[13] Carbon atoms in graphite are hybridized to form sp^2 hybrid orbitals and connected by covalent bonds to form a hexagonal ring, developing carbon layers on the plane. These carbon layers are connected by weak van der Waals interaction generated by non-localized π orbitals. Graphite is anisotropic,[14] having low electronic activity within the layers (due to the in-plane covalent bonds) and having high electronic activity between the layers (due to the weak van der Waals forces). This special structural feature makes graphite contain abundant carriers inside, and exhibits excellent conductivity, enabling graphite to be used as electrode material, lubricant, heat transfer material, pencil material, etc.[14–17]

As is shown in Figure 1 and Table 1, seven C1s components of graphite are listed, such as C=C (284.1–284.5 eV), C–C (284.4–285.1 eV), C–H (285.0–285.2 eV), C–O (286.0–287.0 eV), C=O (286.8–288.3 eV), COOH/COOR (288.0–289.5 eV) and π-π^* (290.8–291.3 eV). Ref.[18] has a

CONTACT De Fang fangde@whut.edu.cn School of Materials Science and Engineering, Wuhan University of Technology, Wuhan 430070, PR China.

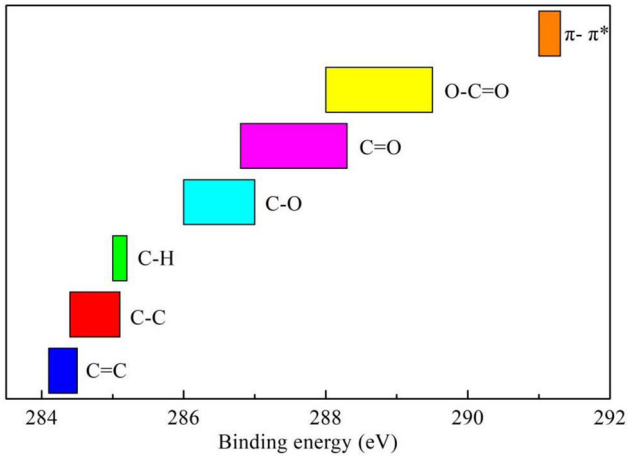

Figure 1. Binding energy range for the C1s components of graphite.

Table 1. Binding energy (eV) for the C1s components of graphite.

Ref.	C=C	C–C	C–H	C–O	C=O	COOH/COOR	π-π^*
[18]	284.1	285.1			287.1	288.1	
[19]		284.4	285.0	286.8		288.5	291.0
[20]		284.5	285.2	286.3	287.7		290.8
[21]	284.5	284.8		286.0	287.0	288.0	
[22]		284.8		287.0	288.3	289.5	291.3

sharp C=C peak whereas the other four samples have strong C–C peak and have no or weaker C=C peak. The sp^2 hybridized carbon is attributed to graphite, and the sp^3 hybridized species indicate amorphous carbon on the membranes surface. Hydrogen and oxygen are the common foreign elements. There are oxygen bonds in all the five samples, indicating the surface of graphite contains oxygen element. C–H bond is observed in Ref.[19,20] while others not. The C–H bond and oxygen-containing bonds are formed due to the presence of edge and defect sites in graphite which provide suitable anchoring sites for the functionalities. Moreover, a single peak is used for C–O and C=O peaks in Ref.[19], as they can't be resolved in the data.

The high-resolution XPS spectra of C1s region for graphite (Iso-molded graphite plate (grade-GM-10, density = 1.82 g/cm^3), purchased from Graphtek LLC) is shown in Figure 2. The deconvoluted C1s peaks show six binding energies of 284.50, 285.15, 286.30, 287.72, 289.00, and 290.81 eV, representing C–C (84.64 at.%), C–H (3.77 at.%), C–O (1.78 at.%), C=O (0.33 at.%), COOH (0.00 at.%)and π-π^* satellite bonds (9.48 at.%), respectively.

2.2. Carbon black

Carbon black is amorphous carbon.[23] As an indispensable raw material in rubber industry, carbon black is commonly used as filler of rubbers in the formulation of adhesives and sealants and in tire fabricating. In addition, it shows a wide range of applications as a pigment for color paste, coating, ink and toner aspects.[24–27] Much work has been carried out to modify the surface of carbon black for enhanced dispersion, increased compatibility and improved performance. And XPS is widely used in observe the changes in surface properties during the modification process.

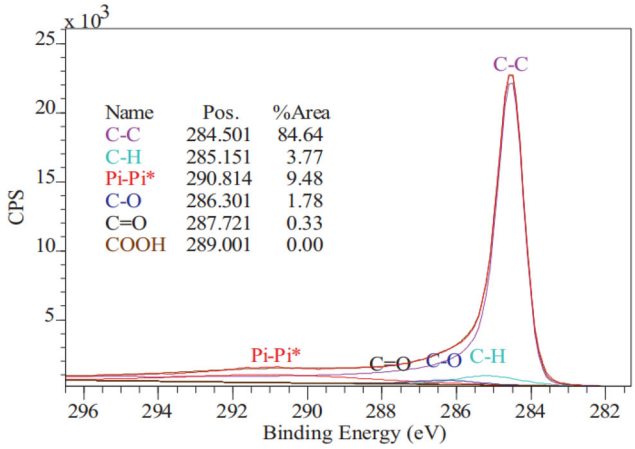

Figure 2. Typical high-resolution XPS spectra in C1s region of graphite.[20]

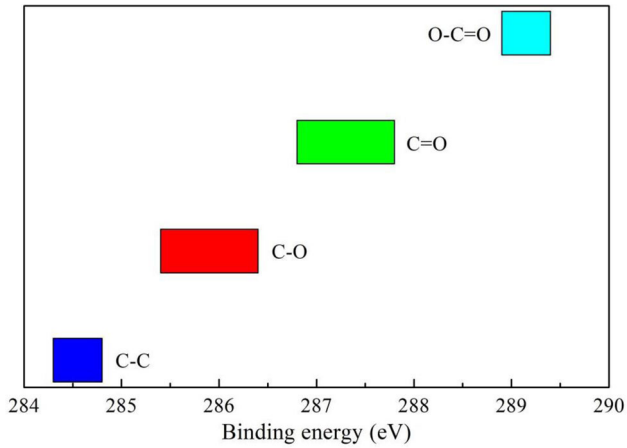

Figure 3. Binding energy range for the C1s components of carbon black.

As is shown in Figure 3 and Table 2, it can be found that the carbon black has four C1s components (C–C, C-O, C=O and COOH/COOR) which have the range of 284.3–284.8 eV, 285.4–286.4 eV, 286.8–287.8 eV, 288.9–289.4 eV, respectively. All five samples have similar fitting peaks with the main sp^3C signal indicating amorphous carbon and three weak oxygen signals indicating oxide contamination. Among the C–O, C=O and O=C–O bonds, the C–O peak is dominant. These oxygen-containing groups are generated due to binding of oxygen to uncompleted carbon bonds on carbon black during synthetic procedure.

Figure 4 shows the detailed fundamental line of C1s of carbon black (Corax N220) which can be decomposed in four signals. The main signal is located at 284.3 eV which corresponds to C-C bond whereas three weak signals appear at 285.4, 286.9 and 288.9 eV that represent C–O, C=O and O–C=O bond, respectively.

2.3. Graphene

Graphene is a two-dimensional carbon nanomaterial with hexagonal honeycomb lattice composed of carbon atoms with sp^2 hybrid orbitals. It is the basic structural unit of carbon materials such as fullerene, carbon nanotubes and graphite. Graphene has become a research hotspot since it

was discovered by Andrei Gem and Konstantin Novoselov in 2004.[32] It is considered as a revolutionary material in the future because of its excellent optical, electrical, and mechanical properties[32–37] and its important application prospects in materials science, micro/nano processing, energy, biomedicine, and drug delivery.[33,38–42]

Graphene can be prepared by mechanical exfoliation,[43] chemical vapor deposition (CVD),[44] thermal exfoliation,[45] epitaxial growth on silicon carbide (SiC) wafer[46,47] and chemical oxidation-reduction method,[48,49] among which chemical oxidation-reduction method is the most commonly used with the product named reduced graphene oxide (rGO). For the chemical oxidation-reduction method, graphene oxide (GO) is prepared by oxidation and exfoliation of graphite, and then it is reduced to graphene by a strong reducing agent. And the modified Hummers method[50,51] is the most favored method to prepare GO. In all this process, XPS can be used to obtain changes in the surface structure of the substances.

The binding energy range for C1s components of GO is shown in Figure 5 and Table 3. There are C=C (284.1-284.7 eV), C–C (284.7–285.4 eV), C–O (285.5-287.0 eV), C=O (286.1–288.0 eV) and COOH/COOR (288.7–289.5 eV) bonds for GO. As there are plenty of oxygen element on the GO surface, the oxygen-containing C1s peaks are comparatively strong. For the three oxygen-containing groups: C–O, C=O, O–C=O, C–O peak dominates them all. Besides, Ref.[50] has a unique main peak of C-O bond while the other four samples have strong peak of C=C bond, which means GO of Ref.[50] has richer oxygen-containing functional groups than the others. Strong oxidants react with water or hydrogen ions to generate active substances like ozone, atomic oxygen radicals or hydroxyl radicals through a series of reactions, selectively oxidizing graphite to generate C–OH and C–O–C groups on the graphene layer. In addition, the oxidants destroy the sp^2 hybrid structure of the graphite, thereby generating C=O and O=C–O groups mostly at the edge of graphene layer.

As for graphene, it has seven possible C1s components, such as C=C (284.3–284.6 eV), C–C (284.9–285.6 eV), C–OH (285.4-286.7 eV), C–O–C (285.6-286.9 eV), C=O (287.9-288.3 eV), COOH/COOR (288.3–289.4 eV) and π-π^* (290.5–291.2 eV) (shown in Figure 6 and Table 4). All the five samples have the extremely sharp sp^2C peak (C=C) and several weak oxygen-containing C1s peak. Ref.[56,58,59] have sp^3C peak (C-C) while the other two don't have that, indicating that the surfaces of the three graphene contain amorphous carbon. As the graphene of Ref.[54,57,58] are prepared by chemically or thermally reduction, the presence of oxygen-containing groups of these three samples represents incomplete reduction from GO to rGO. Graphene of Ref.[56]

Table 2. Binding energy (eV) for the C1s components of carbon black.

Ref.	C-C	C-O	C=O	COOH/COOR
[28]	284.8	286.2	287.7	289.3
6]	284.3	285.4	286.9	288.9
[29]	284.4	285.9	287.4	288.9
[30]	284.6	286.4	287.8	288.9
[31]	284.6	285.4	286.8	289.4

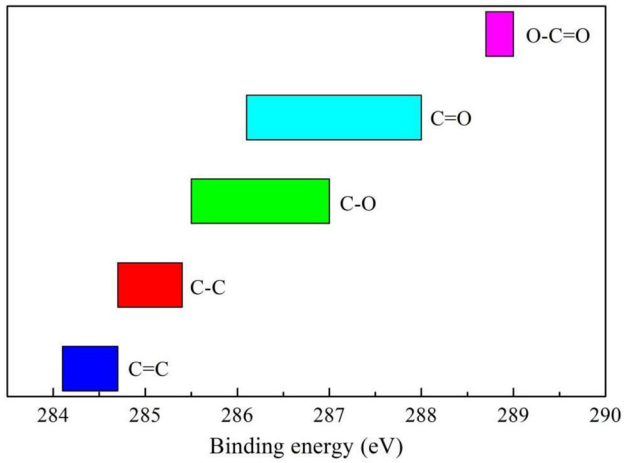

Figure 5. Binding energy range for the C1s components of GO.

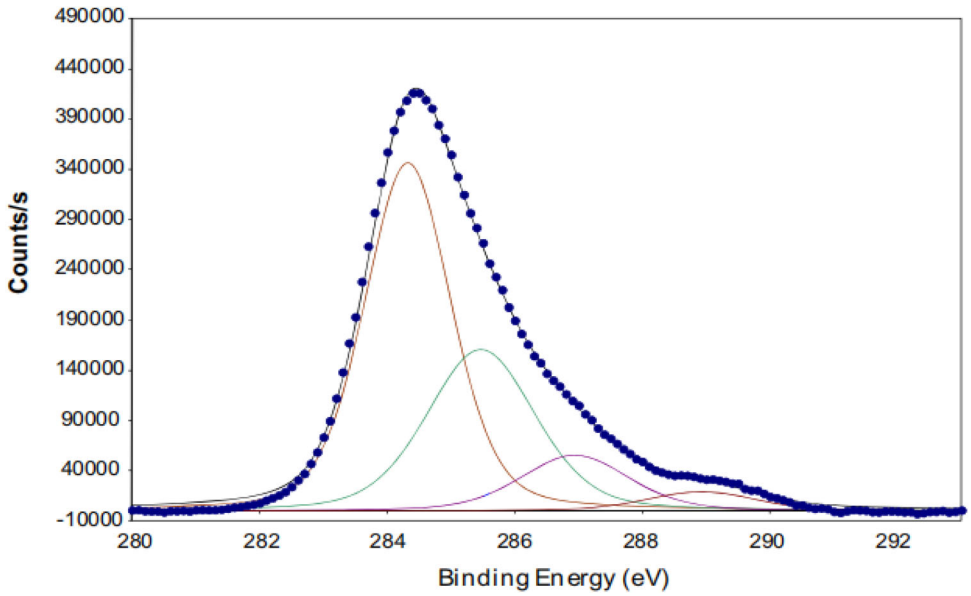

Figure 4. Typical high-resolution XPS spectra in C1s region of carbon black.[6]

Table 3. Binding energy (eV) for the C1s components of GO.

			C-O			
Ref.	C=C	C-C	C-OH	C-O-C	C=O	COOH/COOR
[52]	284.1	284.7		285.5	286.1	288.7
[53]	284.7		287.0		288.0	289.2
[50]	284.6		286.6		287.8	289.5
[54]	284.5		285.9	286.6	287.5	288.9
[55]	284.4	285.4	286.3		288.0	289.0

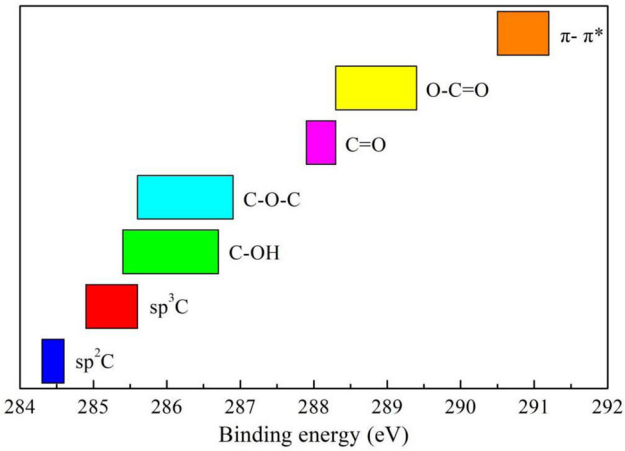

Figure 6. Binding energy range for the C1s components of graphene.

Table 4. Binding energy (eV) for the C1s components of graphene.

Ref.	C=C	C–C	C–OH	C–O–C	C=O	COOH/COOR	π-π*
[56]	284.3	285.3		286.5	287.9		291.2
[54]	284.5		285.4	286.6	288.3		290.5
[57]	284.6			285.6	288.2	289.4	
[58]	284.6	284.9	285.9	286.9	288.2	289.3	290.6
[59]	284.5	285.6	286.7			288.3	

is prepared by electrochemical exfoliation method. The C–O–C and C=O groups are derived from oxidized carbon contamination during the electrolysis process. Graphene of Ref.[59] is prepared by CVD method. And the C–OH peak of Ref.[59] is much stronger compared to the others. The C-OH and O=C-O bonds are attributed to adsorption contamination during transfer process.

Figure 7a shows high-resolution XPS spectra of C1s region of GO produced by modified Hummers method. The deconvoluted C1s peaks appear at 284.5, 285.9, 286.6, 287.5, and 288.9 eV, assigned to C=C, C–OH, C–O–C, C=O, HO–C=O bonds, respectively. And the C1s core level XPS spectra of thermally reduced graphene oxide at 400 °C are shown in Figure7b. Five peaks appear at 284.5, 285.4, 286.6, 288.3 and 290.5 eV, which are attributed to the C=C, C-OH, C-O-C, and C=O and π-π* satellite groups, respectively. Compared to GO, a new peak belonging to π-π* shakeup satellite appears in rGO. In addition, the peaks belonging to oxygen-containing functional groups decreases sharply, indicating the rGO is reduced in a very high degree.

2.4. Carbon nanotubes

Carbon nanotubes (CNTs), one-dimensional nanomaterials, are mainly composed of carbon atoms arranged in a hexagonal shape to form a coaxial circular tube with several layers to dozens of layers which keep a fixed distance of about 0.34 nm[60] between layers. CNTs have high modulus, strength, flexibility, melting point, hydrogen storage capacity, electrical and thermal conductivity,[61–65] illustrating broad applications in supercapacitor, catalyst carrier, composite, electromagnetic interference shielding, conductive, hydrogen storage materials, etc.[66–70] CNTs can be regarded as rolled from graphene sheets, so they can be divided into single-walled carbon nanotubes (SWCNTs) and multi-walled carbon nanotubes (MWCNTs) according to the number of graphene sheets. It is easy to capture various defects between layers of MWCNTs. However, compared with MWCNTs, SWCNTs have a smaller diameter distribution range, fewer defects, and higher uniformity.

The C1s components of CNTs are listed in Figure 8 and Table 5. C=C (284.1–284.6 eV), C–C (284.7–286.0 eV), C–O (285.8–286.8 eV), C=O (287.6–288.9 eV), carbonates (288.3 eV) and π-π* (290.4–291.1 eV) peaks are related to the CNTs. Ref.[72] only have two peaks belonging to C=C and C–C bonds whereas the others also have oxygen-containing C1s peaks, indicating that Ref.[72] has no surface oxidized carbon contamination while others have. Meanwhile, Ref.[75] has a unique peak at 288.3 eV, which is associated with carbonates. The presence of oxygen-containing groups can be explained by the uncompleted or defected carbon bonds on the CNTs which the oxygen (also contained in surfactant) can bond to during the drying process.

The deconvoluted high-resolution C1s XPS spectra of three kinds of SWCNTs are shown in Figure 9, illustrating (a) bare buckypaper (BP) prepared from single-wall carbon nanotubes (SWCNT BP), (b) SWCNT BP with incorporated diamond nanoparticles (DNPs) and (c) SWCNT BP ingrown/overgrown with nanocrystalline diamond (NCD). The C1s peak of SWCNT BP and SWCNT BP/DNPs is calibrated on 284.6 eV, which corresponds to the sp^2 carbon phase. Peak positions of these two SWCNTs BP are sp^2 C (284.6 eV), sp^3 C (285.2 eV), C-O (286.8 eV), C=O (288.9 eV) and π-π* shakeup feature (291.0 eV). As for SWCNT BP/NCD, the C1s peak is located at 285.1 eV referenced to the sp^3 carbon phase. The deconvoluted C1s XPS spectra of SWCNT BP/NCD, shown in Figure 9c, is fitted to peaks with binding energies of 284.2, 285.1, 286.1, 287.6 eV that are attributed to the sp^2 C, sp^3 C, C-O and C=O bonds, respectively. Compared with SWCNT BP and SWCNT BP/DNPs, the sp^3 phase of SWCNT BP/NCD increases rapidly, and the sp^2 phase of that decreases sharply. In addition, the oxygen bond concentration drops obviously. Besides, the signal of π-π* satellite completely disappeared in the SWCNT BP/NCD. These changes indicate that a sufficiently thick diamond film is formed on the SWCNT BP/NCD substrate. After diamond growth, super-hydrophobic property is greatly enhanced due to reduction in oxygen concentration and hydrophilic functional groups on SWCNT surface.

2.5. Carbides

Carbides can be divided into metal carbides (Titanium Carbide (TiC), calcium carbide (CaC_2), chromium carbide (Cr_4C_3), vanadium carbide (VC), tantalum carbide (TaC),

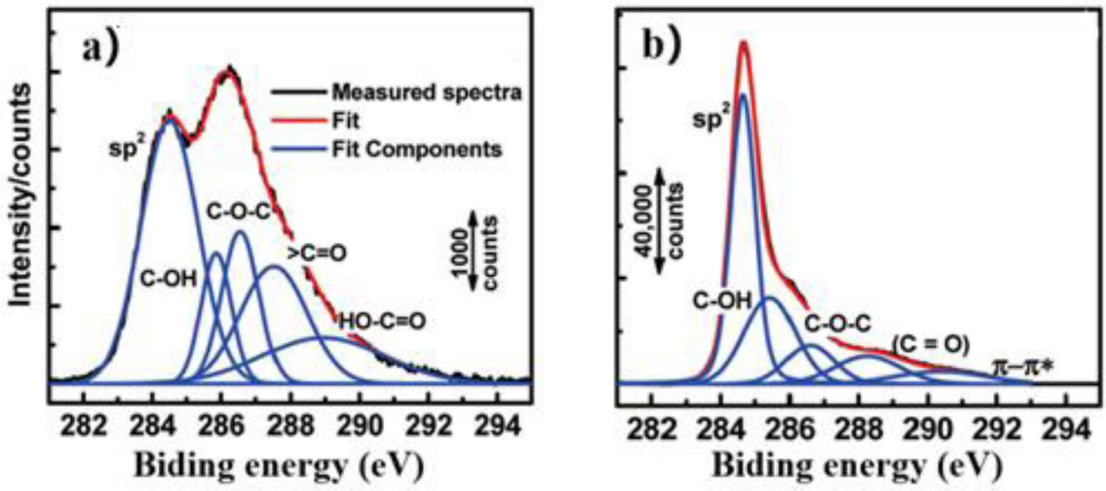

Figure 7. Typical high-resolution XPS spectra in C1s region of (a) GO and (b) graphene.[54]

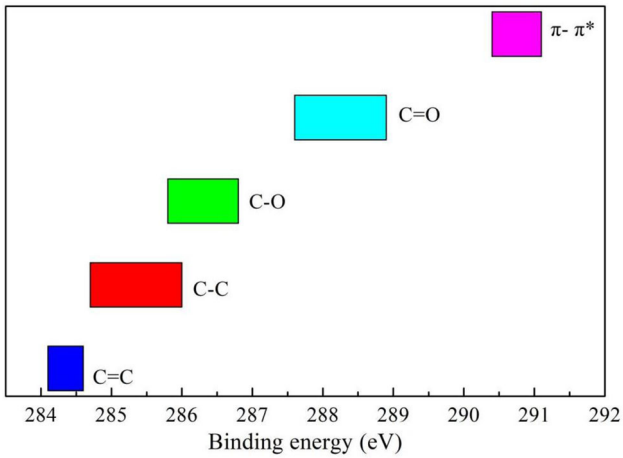

Figure 8. Binding energy range for the C1s components of CNTs.

Table 5. Binding energy (eV) for the C1s components of CNTs.

Ref.	C=C	C–C	C–O	C=O	carbonates	π-π^*
[71]	284.6	285.2	286.8	288.9		291.0
[72]	284.5	285.6				
[73]	284.5	286.0		287.6		291.1
[74]	284.5	284.7	285.8	288.0		
[75]	284.1	285.5	286.7		288.3	290.4

and zirconium carbide (ZrC), Tungsten carbide (WC), etc) and nonmetal carbides (boron carbide (B_4C), silicon carbide (SiC), and the like) according to their attributes. Among the metal carbides, transition metal carbides (TMCs) attract tremendous scientific and technological interest due to their excellent properties including chemical inertness, high hardness, high melting points, and metallic conductivity.[76–80] And as a typical TMC, TiC is a major wear-resistant coating material because of its high hardness, strength and rigidity, outstanding wear resistance, corrosion resistance, heat-resistance, and low friction coefficient.[81–83] To obtain the detailed information about the surface chemistry of TiC, XPS analysis is inevitable.

As is shown in Figure 10 and Table 6, C–Ti (281.7–282.1 eV), C–C (284.3–284.9 eV) and C–O (288.8 eV) peaks take place for the C1s components of TiC. All the five samples have peaks belonging to C–Ti bond and C–C bond of amorphous carbon. Specifically, Ref. [86] has a weak peak at 288.8 eV due to C–O bond of oxygen contamination during air exposure. Figure 11 shows high-resolution XPS C1s region spectra of TiC. The deconvoluted C1s peaks with binding energies of 282.1 and 284.3 eV, correspond to the C–Ti and C–C bonds, respectively.

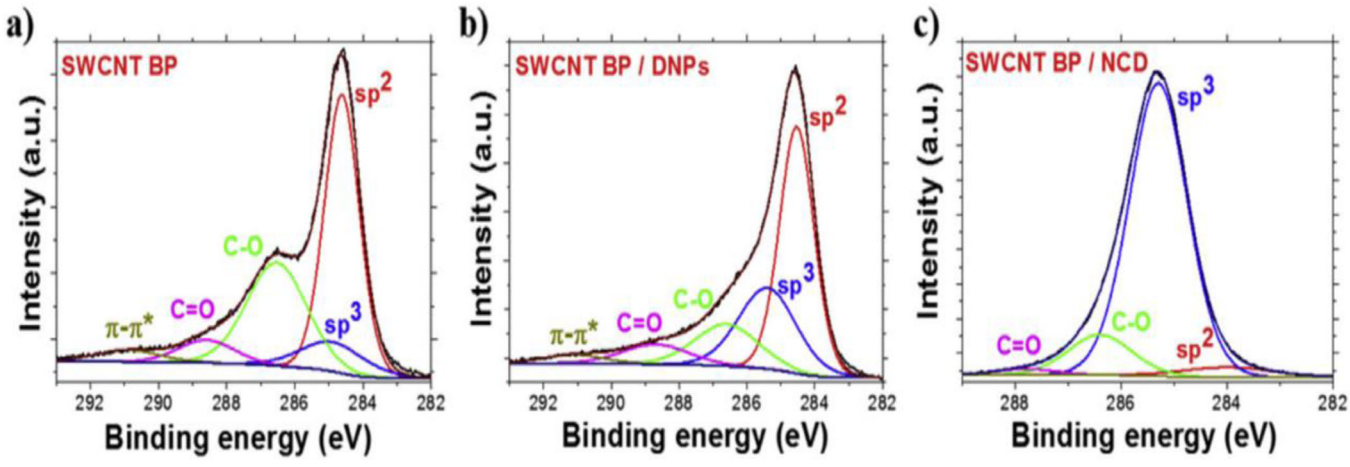

Figure 9. The deconvoluted C1s XPS spectra of (a) SWCNT BP, (b) SWCNT BP/DNPs and (c) SWCNT BP/NCD.[71]

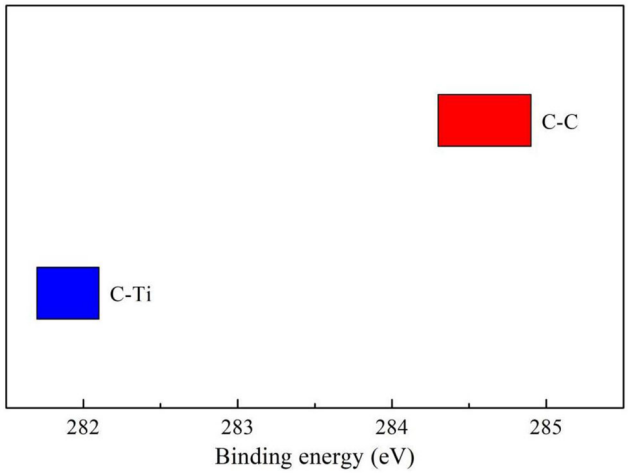

Figure 10. Binding energy range for the C1s components of TiC.

Table 6. Binding energy (eV) for the C1s components of TiC.

Ref.	C-Ti	C–C	C–O
[81]	282.1	284.6	
[84]	281.7	284.5	
[85]	282.1	284.3	
[86]	281.9	284.9	288.8
[87]	281.9	284.8	

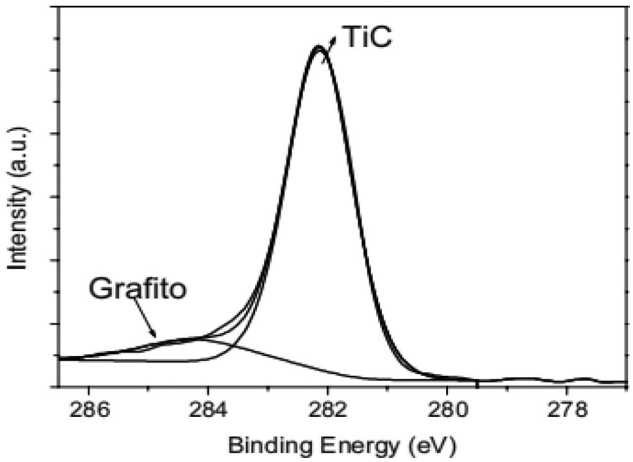

Figure 11. The deconvoluted C1s XPS spectra of TiC.[85]

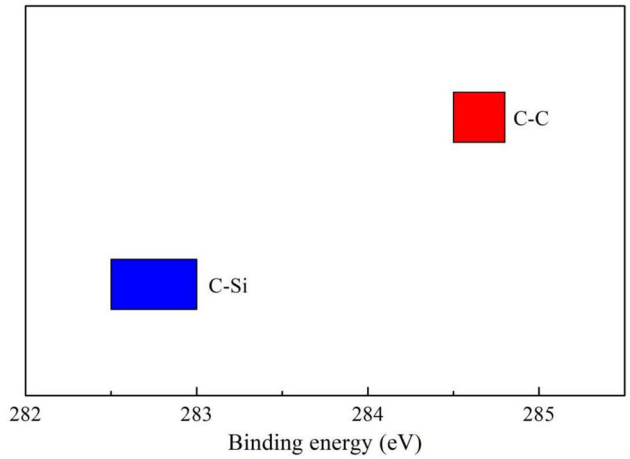

Figure 12. Binding energy range for the C1s components of SiC.

Table 7. Binding energy (eV) for the C1s components of SiC.

Ref.	C–Si	C–C	C–O
[93]	283.0	284.6	
[94]	282.5	284.5	286.1
[95]	282.9	284.7	
[96]	282.6	284.8	286.1
[97]	283.0	284.8	

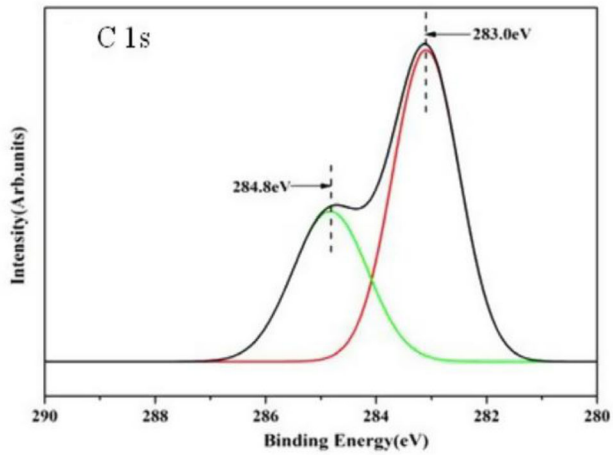

Figure 13. C1s core levels in XPS spectra of SiC.[98]

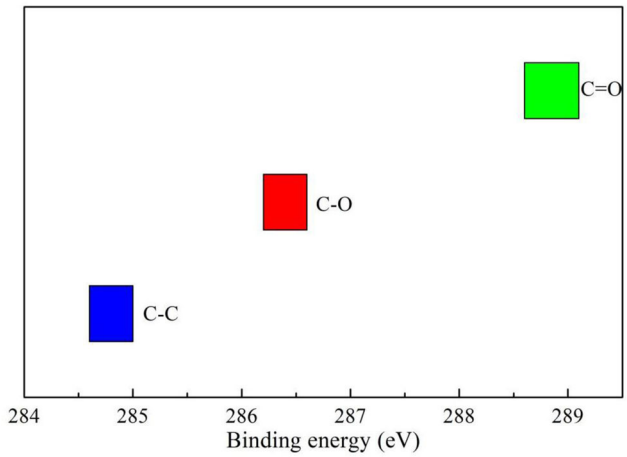

Figure 14. Binding energy range for the C1s components of PET.

Table 8. Binding energy (eV) for the C1s components of PET.

Ref.	C–C	C–O	C=O	π-π^*
[104]	284.7	286.3	288.7	
[105]	284.6	286.5	288.9	
[106]	285.0	286.5	289.1	
[107]	284.6	286.2	288.6	
[108]	285.0	286.6	289.0	291.8

Silicon carbide (SiC), characterized by high breakdown voltage, electron mobility, wear resistance, corrosion resistance, chemical inertness, thermal conductivity and good hardness, is widely used in functional ceramics, advanced refractory materials, abrasives, wide band gap semiconductor and metallurgical raw materials.[88–92] XPS is very useful in the research of oxidation mechanism, metallization mechanism, doping mechanism, and the growth of SiC.

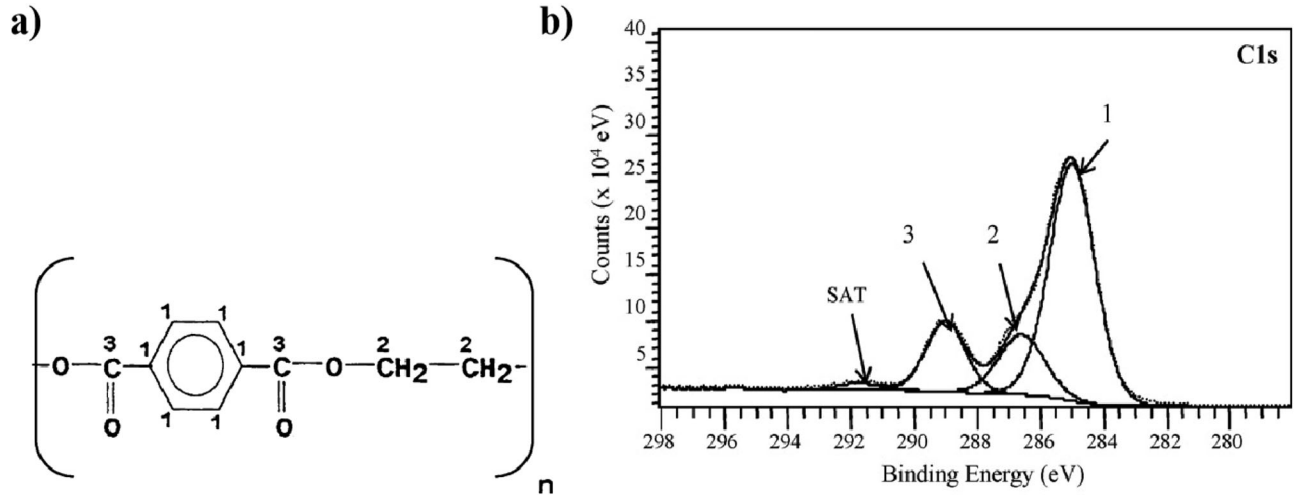

Figure 15. (a) structure and (b) typical high-resolution XPS spectra in C1s region of PET.[108]

As is shown in Figure 12 and Table 7, C–Si (282.5–283.0 eV), C–C (284.5–284.8 eV) and C–O (286.1 eV) bonds of C1s components on the surface of SiC. Except for the C-Si bond, all these five samples have peaks assigned to C–C bonds of adventitious carbon. And it can be observed that Ref.[94,96] have peaks corresponding to C–O bonds of oxygen contamination whereas others don't have. The surface of SiC can be oxidized because of the milling process, the synthetic procedure or the other cases.[94] For crystalline SiC, the typical binding energy of C1s is 280.7–283.0 eV.[94] Figure13 shows that the C atom of SiC is in different oxidation states. In this case, the energy binding peaks are located at 283.0 eV and 284.8 eV, assigned to C–Si and C–C bond, respectively.

2.6. Polymers (PET)

Polymers which play important role in variety of industries are everywhere in human society. According to Ref.[7], some kinds of polymers (PE, PET, nylon 66 and PVDF films) are exposed in air for different times and tested by XPS, providing the evidence for the conclusion that no adventitious carbon is on the surface of the polymers. Polyethylene terephthalate (PET), a commonly known polymer and the most widely used synthetic polyester over the world, has been extensively applied in a number of different fields such as decorative coatings, packaging, capacitors due to its high tensile strength, hardness, corrosion resistance, thermal resistance, transparency, stability and resistance to UV radiation.[98–103] However, PET has low surface free energy and high chemical inertness,[101] which limits its applications. XPS is an effective tool to obtain the surface information when PET is improved and modified.

The C1s components of PET are listed in Figure 14 and Table 8. C–C (284.6–285.0 eV), C–O (286.2–286.6 eV), C=O (288.6–289.1 eV), and π-π^* (291.8 eV) are observed for PET. Except for Ref.[108] in consideration of π-π^* shakeup satellite, the others have the same C1s components with similar binding energy peaks. The C–O bonds come from aliphatic esters and C=O bonds carboxyl component.

According to Figure 15, there are three kinds of chemical states of C atoms in PET. The first peak with a lower binding energy appearing at 285.0 eV is fitted to C–C bonds of aromatic hydrocarbons echo with C1 structure in Figure15a. The peaks 2 and 3 with binding energies of 286.6 and 289.0 eV are corresponding to C–O bonds of aliphatic esters and C=O bonds of carboxyl component, fitting to C2 and C3 structure respectively. The energy binding peak located at 291.8 eV is assigned to π-π^* shakeup satellite.

3. Conclusion

Carbon materials with special surface properties have been widely used and studied and XPS is one of the most optimum measuring methods with surface sensitivity, so XPS and its use as a chemical imaging tool can provide deep insight about carbon materials and be part of reliability testing for industries. In this paper, the binding energy range of C1s components for graphite, carbon black, graphene oxide, graphene, CNTs, TiC, SiC and PET is concluded. C=C, C–C, C–H, C–O, C=O, COOH/COOR and π-π^* components of graphite are be observed. Carbon black has C–C, C–O, C=O and COOH/COOR bonds. There are C=C, C–C, C–O, C=O and COOH/COOR bonds for GO. As for graphene, it has seven possible C1s components, such as C=C, C–C, C–OH, C–O–C, C=O, COOH/COOR and π-π^*. C=C, C-C, C-O, C=O, carbonates and π- π^*peaks are related to the CNTs. C–Ti, C–C, C–O can be detected on the surface of TiC. Three C1s components of SiC are presented, such as C–Si, C–C, C–O. C–C, C–O, C=O, and π-π^* can be found for the C1s components of PET.

Funding

This work is financially supported by Fundamental Research Funds for the Central Universities (WUT: 2019III015GX).

References

[1] Dekanski, A.; Stevanovic, R.; Nikolic, B. Z.; Jovanovic, V. M.; Stevanovic, J. Glassy Carbon Electrodes I. Characterization and Electrochemical Activation. *Carbon* **2001**, *39*, 1195–1205. DOI: 10.1016/S0008-6223(00)00228-1.

[2] Marrani, A. G.; Coico, A. C.; Giacco, D.; Zanoni, R.; Scaramuzzo, F. A.; Schrebler, R.; Dini, D.; Bonomo, M.; Dalchiele, E. A. Integration of Graphene onto Silicon through Electrochemical Reduction of Graphene Oxide Layers in Non-Aqueous Medium. *Appl. Surf. Sci.* **2018**, *445*, 404–414. DOI: 10.1016/j.apsusc.2018.03.147.

[3] Krasovskii, P. V.; Malinovskaya, O. S.; Samokhin, A. V.; Blagoveshchenskiy, Y. V.; Kazakov, V. A.; Ashmarin, A. A. XPS Study of Surface Chemistry of Tungsten Carbides Nanopowders Produced through DC Thermal Plasma/Hydrogen Annealing Process. *Appl. Surf. Sci.* **2015**, *339*, 46–54. DOI: 10.1016/j.apsusc.2015.02.152.

[4] Mohamed, N. M.; Irshad, M. I.; Abdullah, M. Z.; Saheed, M. S. M. Novel Growth of Carbon Nanotubes on Nickel Nanowires. *Diam. Relat. Mater.* **2016**, *65*, 59–64. DOI: 10.1016/j.diamond.2016.01.026.

[5] Mazzaracchio, V.; Tomei, M. R.; Cacciotti, I.; Chiodoni, A.; Novara, C.; Castellino, M.; Scordo, G.; Amine, A.; Moscone, D.; Arduini, F. Inside the Different Types of Carbon Black as Nanomodifiers for Screen-Printed Electrodes. *Electrochim. Acta* **2019**, *317*, 673–683. DOI: 10.1016/j.electacta.2019.05.117.

[6] Strzemiecka, B.; Voelkel, A.; Donate-Robles, J.; Martin-Martinez, J. M. Assessment of the Surface Chemistry of Carbon Blacks by TGA-MS, XPS and Inverse Gas Chromatography Using Statistical Chemometric Analysis. *Appl. Surf. Sci.* **2014**, *316*, 315–323. DOI: 10.1016/j.apsusc.2014.07.174.

[7] Fang, D.; He, F.; Xie, J.; Xue, L. Calibration of Binding Energy Positions with C1s for XPS Results. *Wuhan Univ. Technol.-Mater. Sci. Ed.* **2020**, *35*, 711–718. DOI: 10.1007/s11595-020-2312-7.

[8] Mohanty, A.; Chakladar, S.; Mallick, S.; Chakravarty, S. Structural Characterization of Coking Component of an Indian Coking Coal. *Fuel* **2019**, *249*, 411–417. DOI: 10.1016/j.fuel.2019.03.108.

[9] Larsen, M. J.; Skou, E. M. ESR, XPS, and Thin-Film RRDE Characterization of Nano Structured Carbon Materials for Catalyst Support in PEM Fuel Cells. *J. Power Sources* **2012**, *202*, 35–46. DOI: 10.1016/j.jpowsour.2011.11.015.

[10] Zhang, Y. Q.; Tamijani, A. A.; Taylor, M. E.; Zhi, B.; Haynes, C. L.; Mason, S. E.; Hamers, R. J. Molecular Surface Functionalization of Carbon Materials via Radical-Induced Grafting of Terminal Alkenes. *J. Am. Chem. Soc.* **2019**, *141*, 8277–8288. DOI: 10.1021/jacs.9b02369.

[11] Torrengo, S.; Canteri, R.; Dell'Anna, R.; Minati, L.; Pasquarelli, A.; Speranza, G. XPS and ToF-SIMS Investigation of Nanocrystalline Diamond Oxidized Surfaces. *Appl. Surf. Sci.* **2013**, *276*, 101–111. DOI: 10.1016/j.apsusc.2013.03.041.

[12] Song, X. N.; Hu, J.; Lin, J.; Wang, S. Y.; Zhang, J. R.; Yang, S. Q.; Ma, Y.; Zhou, Y.; Wang, C. K. Theoretical Study of Nano Onion-like Fullerences C_{20}@C_{80} on XPS and NEXAFS Spectra. *Mol. Phys* **2019**, *117*, 794–803. DOI: 10.1080/00268976.2018.1542167.

[13] Reich, S.; Thomsen, C. Raman Spectroscopy of Graphite. *Philos. Trans. A: Math. Phys. Eng. Sci.* **2004**, *362*, 2271–2288. DOI: 10.1098/rsta.2004.1454.

[14] Chung, D. D. L. Review Graphite. *J. Mater. Sci.* **2002**, *37*, 1475–1489. DOI: 10.1023/A:1014915307738.

[15] Annu, P.; Sharma, S.; Jain, R.; Raja, A. N. Review—Pencil Graphite Electrode: An Emerging Sensing Material. *J. Electrochem. Soc.* **2020**, *167*, 93–101. DOI: 10.1149/2.0012003JES.

[16] Wang, L.; Tieu, A. K.; Zhu, H. T.; Deng, G. Y.; Hai, G. J.; Wang, J.; Yang, J. The Effect of Expanded Graphite with Sodium Metasilicate as Lubricant at High Temperature. *Carbon* **2020**, *159*, 345–356. DOI: 10.1016/j.carbon.2019.12.034.

[17] Zhong, Y. J.; Zhao, B. C.; Lin, J.; Zhang, F.; Wang, H. R.; Zhu, Z. Y.; Dai, Z. M. Encapsulation of High-Temperature Inorganic Phase Change Materials Using Graphite as Heat Transfer Enhancer. *Renew. Energy* **2019**, *133*, 240–247. DOI: 10.1016/j.renene.2018.09.107.

[18] Wollbrink, A.; Ruscher, C. H.; Volgmann, K.; Koch, J.; Breuksch, A.; Tegenkamp, C.; Caro, J. Improved Hydrogen Selectivity of Surface Modified Graphite (SMG) Membranes: Permeation Experiments and Characterisation by micro-Raman Spectroscopy and XPS. *J. Membr. Sci.* **2017**, *528*, 316–325. DOI: 10.1016/j.memsci.2016.12.067.

[19] Blyth, R. I. R.; Buqa, H.; Netzer, F. P.; Ramsey, M. G.; Besenhard, J. O.; Golob, P.; Winter, M. XPS Studies of Graphite Electrode Materials for Lithium Ion Batteries. *Appl. Surf. Sci.* **2000**, *167*, 99–106. DOI: 10.1016/S0169-4332(00)00525-0.

[20] Ashraf, A.; Dastgheib, S. A.; Mensing, G.; Shannon, M. A. Surface Characteristics of Selected Carbon Materials Exposed to Supercritical Water. *J. Supercrit. Fluids* **2013**, *76*, 32–40. DOI: 10.1016/j.supflu.2013.01.017.

[21] Theodosiou, A.; Spencer, B. F.; Counsell, J.; Jones, A. N. An XPS/UPS Study of the Surface/near-Surface Bonding in Nuclear Grade Graphites: A Comparison of Monatomic and Cluster Depth-Profiling Techniques. *Appl. Surf. Sci.* **2020**, *508*, 144764. DOI: 10.1016/j.apsusc.2019.144764.

[22] Al-Gaashani, R.; Najjar, A.; Zakaria, Y.; Mansour, S.; Atieh, M. A. XPS and Structural Studies of High Quality Graphene Oxide and Reduced Graphene Oxide Prepared by Different Chemical Oxidation Methods. *Ceram. Int.* **2019**, *45*, 14439–14448. DOI: 10.1016/j.ceramint.2019.04.165.

[23] Zyla, G. Nanofluids Containing Low Fraction of Carbon Black Nanoparticles in Ethylene Glycol: An Experimental Study on Their Rheological Properties. *J. Mol. Liq.* **2020**, *297*, 111732.

[24] Ghasemi-Kahrizsangi, A.; Neshati, J.; Shariatpanahi, H.; Akbarinezhad, E. Improving the UV Degradation Resistance of Epoxy Coatings Using Modified Carbon Black Nanoparticles. *Prog. Org. Coat.* **2015**, *85*, 199–207. DOI: 10.1016/j.porgcoat.2015.04.011.

[25] Kim, W.; Bae, J.; Eum, C. H.; Jung, J.; Lee, S. Study on Dispersibility of Thermally Stable Carbon Black Particles in Ink Using Asymmetric Flow Field-Flow Fractionation. *Microchem. J.* **2018**, *142*, 167–174. DOI: 10.1016/j.microc.2018.06.035.

[26] Schlick, S.; Fehrenbach, H. Airway Regionspecific Effects of Carbon Black Nanoparticles. *Eur. Resp. J.* **2012**, *40*, 100201.

[27] Bae, J.; Kim, W.; Rah, K.; Jung, E. C.; Lee, S. Application of Flow Field-Flow Fractionation (FlFFF) for Size Characterization of Carbon Black Particles in Ink. *Microchem. J.* **2012**, *104*, 44–48. DOI: 10.1016/j.microc.2012.04.007.

[28] Atif, M.; Bongiovanni, R.; Giorcelli, M.; Celasco, E.; Tagliaferro, A. Modification and Characterization of Carbon Black with Mercaptopropyltrimethoxysilane. *Appl. Surf. Sci.* **2013**, *286*, 142–148. DOI: 10.1016/j.apsusc.2013.09.037.

[29] Pantea, D.; Darmstadt, H.; Kaliaguine, S.; Summchen, L.; Roy, C. Electrical Conductivity of Thermal Carbon Blacks: Influence of Surface Chemistry. *Carbon* **2001**, *39*, 1147–1158. DOI: 10.1016/S0008-6223(00)00239-6.

[30] Zhu, L. J.; Lu, Y. L.; Wang, Y. Q.; Zhang, L. Q.; Wang, W. C. Preparation and Characterization of Dopamine-Decorated Hydrophilic Carbon Black. *Appl. Surf. Sci.* **2012**, *258*, 5387–5393. DOI: 10.1016/j.apsusc.2012.02.016.

[31] Song, P.; Wan, C. Y.; Xie, Y. L.; Zhang, Z.; Wang, S. F. Stepwise Exfoliation of Bound Rubber from Carbon Black Nanoparticles and the Structure Characterization. *Polym. Test* **2018**, *71*, 115–124. DOI: 10.1016/j.polymertesting.2018.08.032.

[32] Novoselov, K. S.; Geim, A. K.; Morozov, S. V.; Jiang, D.; Zhang, Y.; Dubonos, S. V.; Grigorieva, I. V.; Firsov, A. A. Electric Field Effect in Atomically Thin Carbon Films. *Science* **2004**, *306*, 666–669. DOI: 10.1126/science.1102896.

[33] Chae, M. S.; Lee, T. H.; Son, K. R.; Park, T. H.; Hwang, K. S.; Kim, T. G. Electrochemically Metal-Doped Reduced Graphene Oxide Films: Properties and Applications. *J. Mater. Sci. Technol.* **2020**, *40*, 72–80. DOI: 10.1016/j.jmst.2019.09.014.

[34] Jabar, A.; Masrour, R. Magnetic Properties of a Graphene with Alternate Layers. *Superlattices Microstruct.* **2017**, *112*, 541–553. DOI: 10.1016/j.spmi.2017.10.013.

[35] Isacsson, A.; Cummings, A. W.; Colombo, L.; Colombo, L.; Kinaret, J. M.; Roche, S. Scaling Properties of Polycrystalline Graphene: A Review. *2D Mater.* **2016**, *4*, 012002. DOI: 10.1088/2053-1583/aa5147.

[36] Deka, M. J.; Chowdhury, D. Surface Charge Induced Tuning of Electrical Properties of CVD Assisted Graphene and Functionalized Graphene Sheets. *J. Mater. Sci. Technol.* **2019**, *35*, 151–158. DOI: 10.1016/j.jmst.2018.09.017.

[37] Xu, S. G.; Chu, C. L.; Ju, M. T.; Shao, C. F. Macroscale Tribological Properties of Fluorinated Graphene. *Appl. Surf. Sci.* **2018**, *432*, 190–195.

[38] Lee, G. H.; Cooper, R. C.; An, S. J.; Lee, S.; van der Zande, A.; Petrone, N.; Hammerberg, A. G.; Lee, C. G.; Crawford, B.; Oliver, W.; et al. High-strength chemical-vapor-deposited graphene and grain boundaries. *Science* **2013**, *340*, 1073–1076. DOI: 10.1126/science.1235126.

[39] Xu, H. F.; Ma, L. B.; Jin, Z. Nitrogen-Doped Graphene: Synthesis, Characterizations and Energy Applications. *J. Energy Chem.* **2018**, *27*, 146–160. DOI: 10.1016/j.jechem.2017.12.006.

[40] Nag, A.; Mitra, A.; Mukhopadhyay, S. C. Graphene and Its Sensor-Based Applications: A Review. *Sens. Actuator A–Phys.* **2018**, *270*, 177–194. DOI: 10.1016/j.sna.2017.12.028.

[41] Das, S.; Sudhagar, P.; Kang, Y. S.; Choi, W. Graphene Synthesis and Application for Solar Cells. *J. Mater. Res.* **2014**, *29*, 299–319. DOI: 10.1557/jmr.2013.297.

[42] Janani, K.; Thiruvadigal, D. J. Density Functional Study on Covalent Functionalization of Zigzag Graphene Nanoribbon through l-Phenylalanine and Boron Doping: Effective Nanocarriers in Drug Delivery Applications. *Appl. Surf. Sci.* **2018**, *449*, 815–822. DOI: 10.1016/j.apsusc.2017.12.159.

[43] Yin, P.; Ma, M. Efficient and Robust Fabrication of Microscale Graphene Drums. *ACS Appl. Nano Mater.* **2018**, *1*, 6596–6602. DOI: 10.1021/acsanm.8b01347.

[44] Guermoune, A.; Chari, T.; Popescu, F.; Sabri, S. S.; Guillemette, J.; Skulason, H. S.; Szkopek, T.; Siaj, M. Chemical Vapor Deposition Synthesis of Graphene on Copper with Methanol, Ethanol, and Propanol Precursors. *Carbon* **2011**, *49*, 4204–4210. DOI: 10.1016/j.carbon.2011.05.054.

[45] Jankovsky, O.; Mazanek, V.; Klímova, K.; Sedmidubsky, D.; Kosina, J.; Pumera, M.; Sofer, Z. Simple Synthesis of Fluorinated Graphene: Thermal Exfoliation of Fluorographite. *Chemistry* **2016**, *22*, 17696–17703. DOI: 10.1002/chem.201604078.

[46] Whelan, P. R.; Panchal, V.; Petersen, D. H.; Mackenzie, D. M. A.; Melios, C.; Pasternak, I.; Gallop, J.; Osterberg, F. W.; Jepsen, P. U.; Strupinski, W.; et al. Electrical Homogeneity Mapping of Epitaxial Graphene on Silicon Carbide. *ACS Appl. Mater. Interfaces* **2018**, *10*, 31641–31647. DOI: 10.1021/acsami.8b11428.

[47] Whitener, K. E.; Sheehan, P. E. Graphene Synthesis. *Diam. Relat. Mat.* **2014**, *46*, 25–34. DOI: 10.1016/j.diamond.2014.04.006.

[48] Moon, I. K.; Lee, J.; Ruoff, R. S.; Lee, H. Reduced Graphene Oxide by Chemical Graphitization. *Nat. Commun.* **2010**, *1*, 73.

[49] Pei, S. F.; Zhao, J. P.; Du, J. H.; Ren, W. C.; Cheng, H. M. Direct Reduction of Graphene Oxide Films into Highly Conductive and Flexible Graphene Films by Hydrohalic Acids. *Carbon* **2010**, *48*, 4466–4474. DOI: 10.1016/j.carbon.2010.08.006.

[50] Yu, H. T.; Zhang, B. W.; Bulin, C. K.; Li, R. H.; Xing, R. G. High-Efficient Synthesis of Graphene Oxide Based on Improved Gummers Method. *Sci. Rep.* **2016**, *6*, 36143.

[51] Marcano, D. C.; Kosynkin, D. V.; Berlin, J. M.; Sinitskii, A.; Sun, Z. Z.; Slesarev, A.; Alemany, L. B.; Lu, W.; Tour, J. M. Improved Synthesis of Graphene Oxide. *ACS Nano.* **2010**, *4*, 4806–4814. DOI: 10.1021/nn1006368.

[52] Rathnayake, R. M. N. M.; Wijayasinghe, H. W. M. A. C.; Pitawala, H. M. T. G. A.; Yoshimura, M.; Huang, H. H. Synthesis of Graphene Oxide and Reduced Graphene Oxide by Needle Platy Natural Vein Graphite. *Appl. Surf. Sci.* **2017**, *393*, 309–315. DOI: 10.1016/j.apsusc.2016.10.008.

[53] Peng, L.; Xu, Z.; Liu, Z.; Wei, Y. Y.; Sun, H. Y.; Li, Z.; Zhao, X. L.; Gao, C. An Iron-Based Green Approach to 1-h Production of Single-Layer Graphene Oxide. *Nat. Commun.* **2014**, *6*, 5716.

[54] Ganguly, A.; Sharma, S.; Papakonstantinou, P.; Hamilton, J. Probing the Thermal Deoxygenation of Graphene Oxide Using High-Resolution in Situ X-Ray-Based Spectroscopies. *J. Phys. Chem. C* **2011**, *115*, 17009–17019. DOI: 10.1021/jp203741y.

[55] Malinsky, P.; Mackova, A.; Miksova, R.; Kovacikova, H.; Cutroneo, M.; Luxa, J.; Bousa, D.; Strochova, B.; Sofer, Z. Graphene Oxide Layers Modified by Light Energetic Ions. *Phys. Chem. Chem. Phys.* **2017**, *19*, 10282–10291. DOI: 10.1039/C6CP08937B.

[56] Cooper, A. J.; Wilson, N. R.; Kinloch, I. A.; Dryfe, R. A. W. Single Stage Electrochemical Exfoliation Method for the Production of Few-Layer Graphene via Intercalation of Tetraalkylammonium Cations. *Carbon* **2014**, *66*, 340–350. DOI: 10.1016/j.carbon.2013.09.009.

[57] Moon, I. K.; Lee, J.; Lee, H. Highly Qualified Reduced Graphene Oxides: The Best Chemical Reduction. *Chem. Commun. (Camb)* **2011**, *47*, 9681–9683. DOI: 10.1039/c1cc13312h.

[58] Perrozzi, F.; Prezioso, S.; Donarelli, M.; Bisti, F.; De Marco, P.; Santucci, S.; Nardone, M.; Treossi, E.; Palermo, V.; Ottaviano, L. Use of Optical Contrast to Estimate the Degree of Reduction of Graphene Oxide. *J. Phys. Chem. C* **2013**, *117*, 620–625. DOI: 10.1021/jp3069738.

[59] Siokou, A.; Ravani, F.; Karakalos, S.; Frank, O.; Kalbac, M.; Galiotis, C. Surface Refinement and Electronic Properties of Graphene Layers Grown on Copper Substrate: An XPS, UPS and EELS Study. *Appl. Surf. Sci.* **2011**, *257*, 9785–9790. DOI: 10.1016/j.apsusc.2011.06.017.

[60] Kusunoki, M.; Shibata, J.; Rokkaku, M.; Hirayama, T. Aligned Carbon Nanotube Film Self-Organized on a SiC Wafer. *Jpn. J. Appl. Phys.* **1998**, *37*, L605–606. DOI: 10.1143/JJAP.37.L605.

[61] Park, O. K.; Choi, H.; Jeong, H.; Jung, Y.; Yu, J.; Lee, J. K.; Hwang, J. Y.; Kim, S. M.; Jeong, Y.; Park, C. R.; et al. High-Modulus and Strength Carbon Nanotube Fibers Using Molecular Cross-Linking. *Carbon* **2017**, *118*, 413–421. DOI: 10.1016/j.carbon.2017.03.079.

[62] Barnett, C. J.; Gowenlock, C. E.; Welsby, K.; White, A. O.; Barron, A. R. Spatial and Contamination-Dependent Electrical Properties of Carbon Nanotubes. *Nano Lett.* **2018**, *18*, 695–700. DOI: 10.1021/acs.nanolett.7b03390.

[63] Zhang, J.; Terrones, M.; Park, C. R.; Mukherjee, R.; Monthioux, M.; Koratkar, N.; Kim, Y. S.; Hurt, R.; Frackowiak, E.; Enoki, T.; et al. Carbon Science in 2016: Status, Challenges and Perspectives. *Carbon* **2016**, *98*, 708–732. DOI: 10.1016/j.carbon.2015.11.060.

[64] He, T. T.; Li, T.; Huang, Z. X.; Tang, Z. A.; Guan, X. Y. Mechanical and Thermal Properties of the Coaxial Carbon Nanotube@Boron Nitride Nanotube Compossite. *Phys. E* **2019**, *107*, 182–186. DOI: 10.1016/j.physe.2018.11.037.

[65] Zare, Y.; Rhee, K. Y. Analysis of the Connecting Effectiveness of the Interphase Zone on the Tensile Properties of Carbon Nanotubes (CNT) Reinforced Nanocomposite. *Polymers* **2020**, *12*, 896. DOI: 10.3390/polym12040896.

[66] Ansaldo, A.; Bondavalli, P.; Bellani, S.; Castillo, A. E. D.; Prato, M.; Pellegrini, V.; Pognon, G.; Bonaccorso, F. High-Power Graphene-Carbon Nanotube Hybrid Supercapacitors. *ChemNanoMat* **2017**, *3*, 436–446. DOI: 10.1002/cnma.201700093.

[67] Wang, Q.; Wang, H. H.; Zhang, Y. J.; Wen, G. D.; Liu, H. Y.; Su, D. S. Syntheses and Catalytic Applications of the high-N-Content, the Cup-Stacking and the Macroscopic Nitrogen

Doped Carbon Nanotubes. *J. Mater. Sci. Technol.* **2017**, *33*, 843–849. DOI: 10.1016/j.jmst.2017.01.011.

[68] Li, J. T.; Zhang, G. C.; Zhang, H. M.; Fan, X.; Zhou, L. S.; Shang, Z. Y.; Shi, X. T. Electrical Conductivity and Electromagnetic Interference Shielding of Epoxy Nanocomposite Foams Containing Functionalized Multi-Wall Carbon Nanotubes. *Appl. Surf. Sci.* **2018**, *428*, 7–16. DOI: 10.1016/j.apsusc.2017.08.234.

[69] Anikina, E.; Banerjee, A.; Beskachko, V.; Ahuja, R. Li-Functionalized Carbon Nanotubes for Hydrogen Storage: Importance of Size Effects. *ACS Appl. Nano Mater.* **2019**, *2*, 3021–3030. DOI: 10.1021/acsanm.9b00406.

[70] Mokry, G.; Pozuelo, J.; Vilatela, J. J.; Sanz, J.; Baselga, J. High Ampacity Carbon Nanotube Materials. *Nanomaterials* **2019**, *9*, 383. DOI: 10.3390/nano9030383.

[71] Varga, M.; Izak, T.; Vretenar, V.; Kozak, H.; Holovsky, J.; Artemenko, A.; Hulman, M.; Skakalova, V.; Lee, D. S.; Kromka, A. Diamond/Carbon Nanotube Composites: Raman, FTIR and XPS Spectroscopic Studies. *Carbon* **2017**, *111*, 54–61. DOI: 10.1016/j.carbon.2016.09.064.

[72] Lee, S. W.; Lee, B. J.; Oda, T. XPS Investigation and Field Emission Property of Ar Plasma Processed Carbon Nanotubes Films. *Trans. Electr. Electron. Mater.* **2008**, *9*, 52–56. DOI: 10.4313/TEEM.2008.9.2.052.

[73] Soin, N.; Roy, S. S.; Karlsson, L.; McLaughlin, J. A. Sputter Deposition of Highly Dispersed Platinum Nanoparticles on Carbon Nanotube Arrays for Fuel Cell Electrode Material. *Diam. Relat. Mat.* **2010**, *19*, 595–598. DOI: 10.1016/j.diamond.2009.10.029.

[74] Velamakanni, A.; Magnuson, C. W.; Ganesh, K. J.; Zhu, Y. W.; An, J. H.; Ferreira, P. J.; Ruoff, R. S. Site-Specific Deposition of Au Nanoparticles in CNT Films by Chemical Bonding. *ACS Nano.* **2010**, *4*, 540–546. DOI: 10.1021/nn901278t.

[75] Thamaraiselvan, C.; Lerman, S.; Weinfeld-Cohen, K.; Dosoretz, C. G. Characterization of a Support-Free Carbon Nanotube-Microporous Membrane for Water and Wastewater Filtration. *Sep. Purif. Technol.* **2018**, *202*, 1–8. DOI: 10.1016/j.seppur.2018.03.038.

[76] Li, H.; Zhang, L. T.; Zeng, Q. F.; Guan, K.; Li, K. Y.; Ren, H. T.; Liu, S. H.; Cheng, L. F. Structural, Elastic and Electronic Properties of Transition Metal Carbides TMC (TM = Ti, Zr, Hf and Ta) from First-Principles Calculations. *Solid State Commun.* **2011**, *151*, 602–606. DOI: 10.1016/j.ssc.2011.02.005.

[77] Greczynski, G.; Primetzhofer, D.; Hultman, L. Reference Binding Energies of Transition Metal Carbides by Core-Level x-Ray Photoelectron Spectroscopy Free from Ar + Etching Artefacts. *Appl. Surf. Sci.* **2018**, *436*, 102–110. DOI: 10.1016/j.apsusc.2017.11.264.

[78] Chang, Y. H. R.; Yoon, T. L. Effects of Nitrogen Addition and Growth Condition on the Enhanced Mechanical Properties of Transition Metal Carbides TMC (TM = Zr, Hf). *Ceram. Int.* **2020**, *46*, 1124–1136. DOI: 10.1016/j.ceramint.2019.09.081.

[79] Chauhan, M.; Gupta, D. C. Electronic, Mechanical, Phase Transition, and Thermo-Physical Properties of TMC (TM = V, Nb, and Ta): High Pressure ab Initio Study. *Phase Transit.* **2015**, *88*, 1193–1212. DOI: 10.1080/01411594.2015.1044529.

[80] Fu, Z. H.; Zhang, S. H.; Legut, D.; Germann, T. C.; Si, C.; Du, S. Y.; Francisco, J. S.; Zhang, R. F. A Synergetic Stabilization and Strengthening Strategy for Two-Dimensional Ordered Hybrid Transition Metal Carbides. *Phys. Chem. Chem. Phys.* **2018**, *20*, 29684–29692. DOI: 10.1039/C8CP06458J.

[81] Santerre, F.; El Khakani, M. A.; Chaker, M.; Dodelet, J. P. Properties of TiC Thin Films Grown by Pulsed Laser Deposition. *Appl. Surf. Sci.* **1999**, *148*, 24–33. DOI: 10.1016/S0169-4332(99)00139-7.

[82] Shanaghi, A.; Ahangarani, S.; Rouhaghdam, A. R. S.; Chu, P. K. Improved Tribological Properties of TiC with Porous Nanostructured TiO_2 Intermediate Layer. *Mater. Chem. Phys.* **2011**, *131*, 420–424. DOI: 10.1016/j.matchemphys.2011.09.067.

[83] Ono, K.; Wakabayashi, M.; Tsukakoshi, Y.; Abe, Y. Decorative Black TiC*x*O*y* Film Fabricated by DC Magnetron Sputtering without Importing Oxygen Reactive Gas. *Appl. Surf. Sci.* **2016**, *364*, 69–74. DOI: 10.1016/j.apsusc.2015.12.009.

[84] Lewin, E.; Gorgoi, M.; Schäfers, F.; Svensson, S.; Jansson, U. Influence of Sputter Damage on the XPS Analysis of Metastable Nanocomposite Coatings. *Surf. Coat. Technol.* **2009**, *204*, 455–462. DOI: 10.1016/j.surfcoat.2009.08.006.

[85] Benavides, V.; Restrepo, E.; Devia, A. Study of TiN/TiC Bilayers Produced by Plasma Assisted Arc Vacuum at Different Temperatures. *Phys. stat. sol. (c)* **2005**, *2*, 3770–3773. DOI: 10.1002/pssc.200461828.

[86] Zoita, N. C.; Braic, V.; Danila, M.; Vlaicu, A. M.; Logofatu, C.; Grigorescu, C. E. A.; Braic, M. Influence of Film Thickness on the Morphological and Electrical Properties of Epitaxial TiC Films Deposited by Reactive Magnetron Sputtering on MgO Substrates. *J. Cryst. Growth* **2014**, *389*, 92–98. DOI: 10.1016/j.jcrysgro.2013.11.076.

[87] Rist, O.; Murray, P. T. Growth of TiC Films by Pulsed Laser Evaporation (PLE) and Characterization by XPS and AES. *Fresenius. J. Anal. Chem.* **1991**, *341*, 360–364. DOI: 10.1007/BF00321937.

[88] Santoni, A.; Frycek, R.; Castrucci, P.; Scarselli, M.; De Crescenzi, M. XPS and STM Study of SiC Synthesized by Acetylene and Disilane Reaction with the Si(1 0 0)2 x 1 Surface. *Surf. Sci.* **2005**, *582*, 125–136. DOI: 10.1016/j.susc.2005.03.010.

[89] Liu, S.; Wang, J. G. Tunable Magnetic Properties of SiC Obtained by Microwave Heating. *J. Alloy Comp.* **2018**, *731*, 369–374. DOI: 10.1016/j.jallcom.2017.09.292.

[90] Seo, J. Y.; Yoon, S. Y.; Niihara, K.; Kim, K. H. Growth and Microhardness of SiC Films by Plasma-Enhanced Chemical Vapor Deposition. *Thin Solid Films* **2002**, *406*, 138–144. DOI: 10.1016/S0040-6090(02)00061-5.

[91] Craciun, D.; Socol, G.; Cristea, D. V.; Stoicanescu, M.; Olah, N.; Balazs, K.; Stefan, N.; Lambers, E.; Craciun, V. Mechanical Properties of Pulsed Laser Deposited Nanocrystalline SiC Films. *Appl. Surf. Sci.* **2015**, *336*, 391–395. DOI: 10.1016/j.apsusc.2014.12.186.

[92] Pyzik, A. J.; Li, C. G. New Design of a Ceramic Filter for Diesel Emission Control Applications. *Int. J. Appl. Ceram. Technol.* **2005**, *2*, 440–451. DOI: 10.1111/j.1744-7402.2005.02045.x.

[93] Shimoda, K.; Park, J. S.; Hinoki, T.; Kohyama, A. Influence of Surface Structure of SiC Nano-Sized Powder Analyzed by X-Ray Photoelectron Spectroscopy on Basic Powder Characteristics. *Appl. Surf. Sci.* **2007**, *253*, 9450–9456. DOI: 10.1016/j.apsusc.2007.06.023.

[94] Wang, Y. Y.; Kusumoto, K.; Li, C. J. XPS Analysis of SiC Films Prepared by Radio Frequency Plasma Sputtering. *Phys. Procedia* **2012**, *32*, 95–102. DOI: 10.1016/j.phpro.2012.03.524.

[95] Kennou, S.; Paloura, E. C.; Kalomiros, J. A.; Ladas, S. Characterization of Ex-Situ Hydrogenated Amorphous SiC Thin Films by X-Ray Photoelectron Spectroscopy. *Appl. Surf. Sci.* **1995**, *90*, 283–287. DOI: 10.1016/0169-4332(95)00075-5.

[96] Mu, F.; Iguchi, K.; Nakazawa, H.; Takahashi, Y.; Fujino, M.; Suga, T. Direct Wafer Bonding of SiC-SiC by SAB for Monolithic Integration of SiC MEMS and Electronics. *ECS J. Solid State Sci. Technol.* **2016**, *5*, 451–456.

[97] Zhan, H. J.; Zhang, N.; Wu, D.; Wu, Z. Q.; Bi, S. X.; Ma, B. J.; Liu, W. Y. Controlled Synthesis of β-SiC with a Novel Microwave Sintering Method. *Mater. Lett.* **2019**, *255*, 126586. DOI: 10.1016/j.matlet.2019.126586.

[98] Chen, J. R.; Wang, X. Y.; Wakida, T. Wettability of Poly(Ethylene Terephthalate) Film Treated with Low-Temperature Plasma and Their Surface Analysis by ESCA. *J. Appl. Polym. Sci.* **1999**, *72*, 1327–1333.

[99] Chen, Z. Z.; Wang, Y. Y.; Cheng, Y. Y.; Wang, X.; Tong, S. W.; Yang, H. T.; Wang, Z. F. Efficient Biodegradation of Highly Crystallized Polyethylene Terephthalate through Cell Surface Display of Bacterial PETase. *Sci. Total Environ.* **2020**, *709*, 136138. DOI: 10.1016/j.scitotenv.2019.136138.

[100] Gorjanc, M.; Mozetic, M.; Primc, G.; Vesel, A.; Spasic, K.; Puac, N.; Petrovic, Z. L.; Kert, M. Plasma Treated Polyethylene Terephthalate for Increased Embedment of UV-Responsive Microcapsules. *Appl. Surf. Sci.* **2017**, *419*, 224–234. DOI: 10.1016/j.apsusc.2017.04.177.

[101] Liu, Y. Q.; Chen, Q. Q.; Du, X. L.; Li, L. Q.; Li, P. Surface Modification of Polyethylene Terephthalate Films by Direct Fluorination. *AIP Adv.* **2018**, *8*, 125333. DOI: 10.1063/1.5066246.

[102] Beeva, D. A.; Borisov, V. A.; Mikitaev, A. K.; Ligidov, M. K.; Beev, A. A.; Barokova, E. B. Controlling the Barrier Properties of Polyethylene Terephthalate. A Review. *Int. Polym. Sci. Technol* **2015**, *42*, 45–52. DOI: 10.1177/0307174X1504200709.

[103] Silva, G. G.; Valente, M. L. D. C.; Bachmann, L.; dos Reis, A. C. Use of Polyethylene Terephthalate as a Prosthetic Component in the Prosthesis on an Overdenture Implant. *Mater. Sci. Eng. C–Biomimetic Supramol. Syst.* **2019**, *99*, 1341–1349.

[104] Shen, T.; Liu, Y.; Zhu, Y.; Yang, D. Q.; Sacher, E. Improved Adhesion of Ag NPs to the Polyethylene Terephthalate Surface via Atmospheric Plasma Treatment and Surface Functionalization. *Appl. Surf. Sci.* **2017**, *411*, 411–418. DOI: 10.1016/j.apsusc.2017.03.149.

[105] Cueff, R.; Baud, G.; Benmalek, M.; Besse, J. P.; Butruille, J. R.; Jacquet, M. X-Ray Photoelectron Spectroscopy Studies of Plasma-Modified PET Surface and Alumina/PET Interface. *Appl. Surf. Sci.* **1997**, *15*, 292–298.

[106] Han, S. H.; Kim, B. J.; Park, J. S. Effects of the Corona Pretreatment of PET Substrates on the Properties of Flexible Transparent CNT Electrodes. *Thin Solid Films* **2014**, *572*, 73–78. DOI: 10.1016/j.tsf.2014.09.066.

[107] Le, Q. T.; Pireaux, J. J.; Verbist, J. J. Surface Modification of PET Films with RF Plasma and Adhesion of in Situ Evaporated A1 on PET. *Surf. Interface Anal.* **1994**, *22*, 224–229. DOI: 10.1002/sia.740220150.

[108] Amor, S. B.; Jacquet, M.; Fioux, P.; Nardin, M. XPS Characterisation of Plasma Treated and Zinc Oxide Coated PET. *Appl. Surf. Sci.* **2009**, *255*, 5052–5061. DOI: 10.1016/j.apsusc.2008.12.067.